Think Positive: Phase Separation Enables a Positively Charged Additive to Induce Dramatic Changes in Calcium Carbonate Morphology

*Bram Cantaert, Yi-Yeoun Kim, Henning Ludwig, Fabio Nudelman, Nico A. J. M. Sommerdijk, and Fiona C. Meldrum**

Soluble macromolecules are essential to Nature's control over biomineral formation. Following early studies where macromolecules rich in aspartic and glutamic acid were extracted from nacre, research has focused on the use of negatively charged additives to control calcium carbonate precipitation. It is demonstrated that the positively charged additive poly(allylamine hydrochloride) (PAH) can also cause dramatic changes in calcite morphologies, yielding thin films and fibers of $CaCO_3$ analogous to those produced with poly(aspartic acid) via a so-called PILP (polymer-induced liquid precursor) phase. The mechanism by which PAH induces these effects is investigated using a range of techniques including cryo transmission electron microscopy (TEM), Raman microscopy, and thermogravimetric analysis, and the data show that hydrated $Ca^{2+}/PAH/CO_3^{2-}$ droplets initially form in solution, before coalescing and ultimately crystallizing to give calcite, together with small quantities of vaterite. It is suggested that it is the initial formation of hydrated $Ca^{2+}/PAH/CO_3^{2-}$ droplets that is key to this process, rather than a specific polymer/mineral interaction. These results are discussed in terms of their relevance to biomineralization processes and highlight the opportunity for using counter-ion-induced phase separation of polyelectrolytes as a method for generating minerals with non-crystallographic morphologies.

1. Introduction

The properties of crystalline materials are defined by many factors including their composition, polymorph, size, shape, orientation, and crystallinity. The ultimate goal in crystal synthesis is therefore to achieve selectivity over these features. Of the approaches investigated, biomimetic strategies, which take inspiration from the ways in which organisms direct the formation of biominerals such as bones, teeth and seashells, are some of the most promising.[1] Although prepared under ambient conditions, biogenic crystals display many remarkable features such as complex morphologies that are entirely disparate from the regular, geometric forms of their synthetic counterparts.[2] Exquisite control is also demonstrated over polymorph, such that an abrupt transition can be achieved from the calcite to aragonite polymorphs of calcium carbonate in the shells of mollusks.[3]

While Nature employs many strategies to control the formation of biominerals, it is the use of soluble macromolecules that has received the most attention.[1,4] This is in part because this process is easy to mimic; indeed, soluble additives provide one of the most common methods for controlling crystallization. Historically, there has also been an overriding ethos that certain key protein sequences are responsible for controlling crystal polymorph,[5,6] morphology, and texture,[7] which has led to a sustained effort to extract and characterize biomacromolecules associated with biominerals.[8–13] From the earliest studies, the biomacromolecules occluded within calcium carbonate biominerals were identified as highly acidic, being rich in aspartic and glutamic acid.[14–18] This then inspired over forty years of experiments using molecular analogues in the form of negatively charged Langmuir monolayers[19] and self assembled monolayers (SAMs),[20] and as negatively charged small soluble organic additives,[21] polymers,[22–24] and block copolymers.[25] Notably, poly(aspartic acid) (PAsp) and poly(acrylic acid) (PAA) were found to be effective in stabilizing a so-called PILP (polymer-induced liquid precursor) phase, which can act as a precursor to amorphous calcium carbonate (ACC).[26] Interest in ACC is currently significant following the realization that in many cases, calcium carbonate biomineralization proceeds via an ACC precursor phase.[27] Further, that PILP possesses a number of unique properties, such as the ability to penetrate into small pores, has led to the suggestion that an analogous phase may participate in the formation of biogenic ACC.[26]

While this focus on negatively charged organic additives has yielded many important results, it has left the potential of alternative additives less explored. Indeed, examination of the amino

B. Cantaert, Dr. Y.-Y. Kim, H. Ludwig, Prof. F. C. Meldrum
School of Chemistry
University of Leeds
Woodhouse Lane, Leeds, LS2 9JT, UK
E-mail: F.Meldrum@leeds.ac.uk
Dr. F. Nudelman, Dr. N. A. J. M. Sommerdijk
Laboratory of Materials and Interface Chemistry
Eindhoven University of Technology
P. O. Box 513, 5600 MB Eindhoven, The Netherlands

DOI: 10.1002/adfm.201102385

acid sequences of mineralization directing biomacromolecules shows that in addition to aspartic and glutamic acid, the basic amino acids, lysine and arginine, are also common. Further, the terminal sequences of nacre macromolecules can exhibit either a net negative or positive charge.[13] Recent modelling results have also shown that arginine residues are the most important binders of the chicken eggshell protein ovocleidin-17 to calcite.[28] Here, we explore the influence of the polyelectrolyte poly(allylamine hydrochloride), $[-CH_2CH(CH_2NH_2 \cdot HCl)-]_n$ (PAH), which exhibits a net positive charge at the selected working conditions, on calcium carbonate precipitation. Positively charged organic additives have received far less attention in the literature than their negatively charged counterparts, and the majority of the studies describe only minor changes in $CaCO_3$ precipitation. As exceptions to this rule, a few polymers with amine side-groups have been reported to stabilize vaterite.[29,30] The data presented here run somewhat counter to these results and conclusively show that positively charged organic additives cannot only stabilize vaterite, but that they can also induce strong morphological changes in calcite. This demonstrates that acidic organic additives are not unique in this behavior.

2. Results

The influence of PAH on calcium carbonate precipitation was apparent upon studying the mineral deposited on a glass slide placed vertically in the reaction solution. The $CaCO_3$ precipitated could be characterized as a function of its position relative to the gas/water interface. The results were compared with control experiments carried out under identical conditions but in the absence of PAH in which calcite rhombohedra, together with a small percentage of vaterite spherules, were distributed over the glass substrate. By comparison, thin films of $CaCO_3$ deposited on the glass slide in the presence of PAH, whose microstructures depended on their location relative to the solution surface. The substrate immersed well into the solution was coated with a continuous, extremely uniform thin film of calcium carbonate (**Figure 1**a), which was typically ≈1 μm in thickness (Figure 1a, inset). Structural investigation of this film showed that it comprised 10–100 μm domains, each of which was polycrystalline in structure, as demonstrated by characteristic Maltese cross patterns when viewed by polarized optical microscopy (POM). Raman microscopy showed that the films were principally calcite (Figure 1b). Some domains were also viewed that appeared significantly brighter than the background (arrow in Figure 1a), and these were identified as vaterite by Raman microscopy (Figure 1b). The film formed on the substrate close to the air/water interface, in contrast, comprised a mosaic of large single crystal domains approximately 50–100 μm in size (Figure 1c), as shown by their uniform contrast and optical extinction under POM (Figure 1c and Supporting Information Figure S1). They were identified as calcite using Raman microscopy.

In addition to supporting the formation of crystalline $CaCO_3$ films, the PAH also induced the growth of fibers of $CaCO_3$. These were only associated with the polycrystalline films and started to develop after deposition of the film. The fibers were generally in the order of 1–2 μm in width, although

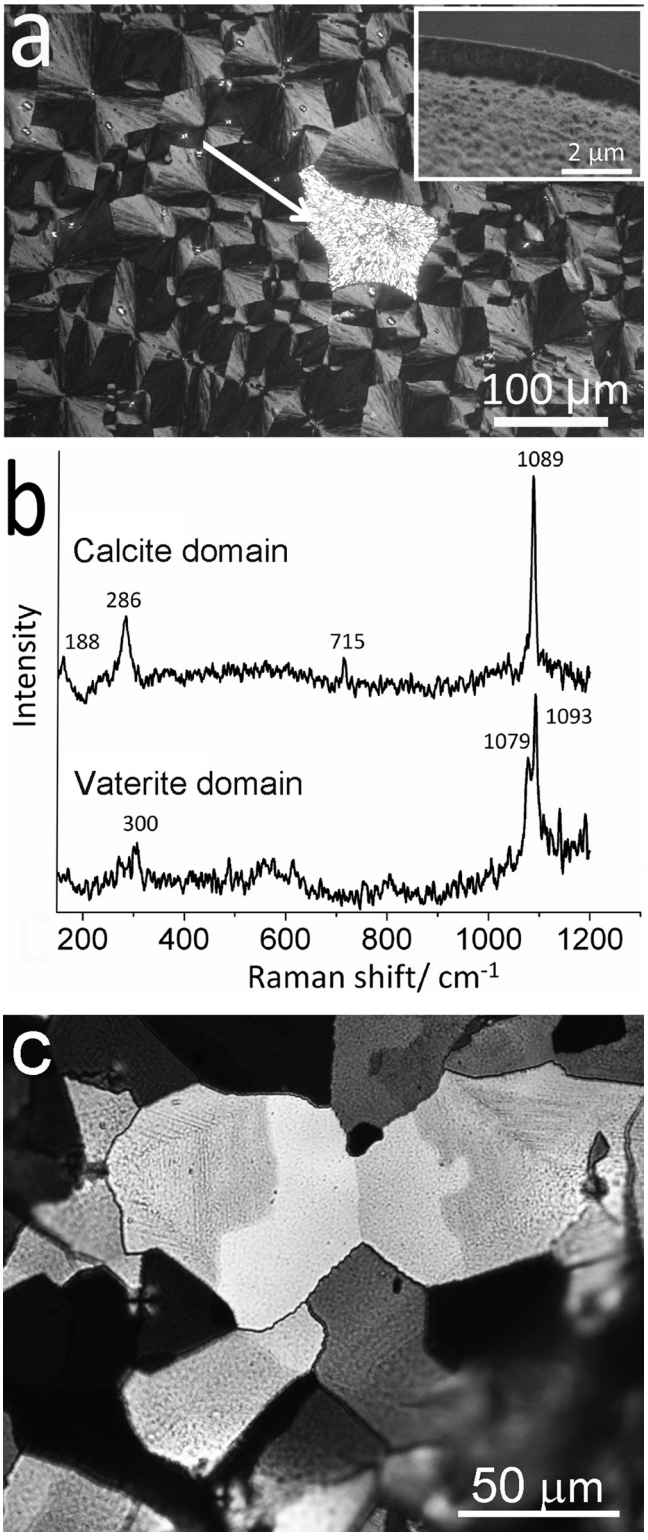

Figure 1. a) POM image of a polycrystalline calcium carbonate thin film formed on a substrate immersed well into the solution, where a small domain of vaterite is indicated with an arrow. The inset shows an scanning electron microscopy (SEM) image of the film in cross section. b) Raman spectra of calcite and vaterite domains in this film. c) POM image of a thin film of single crystal calcite domains deposited on the substrate adjacent to the air/water interface.

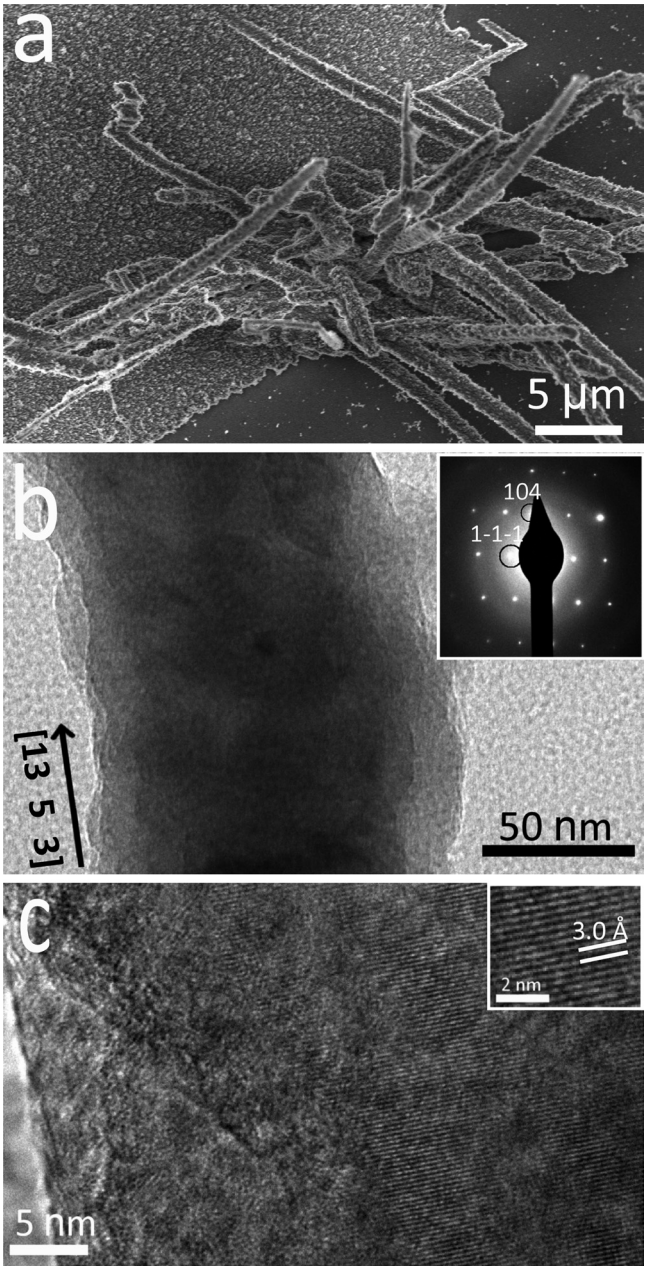

Figure 2. Calcium carbonate fibers formed on the polycrystalline thin films. a) SEM image of the fibers and b) TEM image of an individual fiber, where the inset shows a SAED pattern demonstrating that this fiber is a single crystal of calcite and has a zone axis of [4 5 –1]. An arrow indicates the [13 5 3] direction along the long axis of the fiber. c) An HRTEM image of the fiber shown in (b) showing continuous {104} lattice fringes that terminate in the low-density surface layer.

thinner fibers were also observed (**Figure 2**a). Characterization of thinner fibers using selected area electron diffraction (SAED) and high-resolution transmission electron microscopy (HRTEM) showed that each was a single crystal of calcite. A typical single crystal type SAED pattern is shown as an inset in Figure 2b and corresponds to a [4 5 –1] zone axis and HRTEM of the same fiber showed continuous fringes that corresponded to {104} planes of calcite (Figure 2c). The long axis of this fiber corresponds to the [13 5 3] direction, and analysis of a number of fibers showed no preferential axis. Interestingly, the TEM images of the fibers also show that they are coated with a less dense surface coating (Figure 2b,c). That the lattice fringes did not persist into this coating suggests that it is amorphous, which would be consistent with an extrusion of polymer during crystallization, thereby creating an ACC phase too rich in polymer to crystallize. A similar amorphous layer has also been observed surrounding the aragonite platelets present in mollusk nacre, an effect which was again attributed to their formation via a polymer-stabilized ACC phase.[31] Unfortunately, efforts to determine the elemental composition of the coating on the fibers using energy-dispersive X-ray analysis (EDX) were unsuccessful, due to its small thickness. Similar fibers have been observed in the $CaCO_3$/PAA system,[32] where it was suggested that they formed via a solution-precursor-solid (SPS) mechanism, which is many ways analogous to the vapor-liquid-solid (VLS) and solution-liquid-solid (SLS) mechanisms identified to lead to the formation of many nanowires.[33]

The mechanism by which PAH directs the formation of $CaCO_3$ thin films is intriguing, especially given that most positively charged organic additives exert little influence on calcium carbonate precipitation. The early stages of precipitation of calcium carbonate in the presence of PAH were therefore investigated using a range of methods. PAH is known to undergo microphase separation in the presence of carbonate ions (and a range of other anions[34]) due to the formation and coexistence of $R–NH_3^+$ and $R–NHCO_2^-$ groups in the pH range 7.4 to 10.[35] Indeed, the amine groups on PAH are expected to be 50% protonated at pH 9.5, the working pH value of the precipitation experiments.[36] The microphase separation was confirmed here, and our results also suggest that this still occurred when Ca^{2+} cations were also present in the reaction solution. Droplets, which were seen to condense into thin films, were observed at early reaction times using optical microscopy, which is indicative of phase separation and liquid-like behavior (**Figure 3**). Solutions became turbid both on diffusion of ammonium carbonate vapor into a Ca^{2+}/PAH solution and when Ca^{2+} ions were slowly added to a Na_2CO_3/PAH solution. In the latter

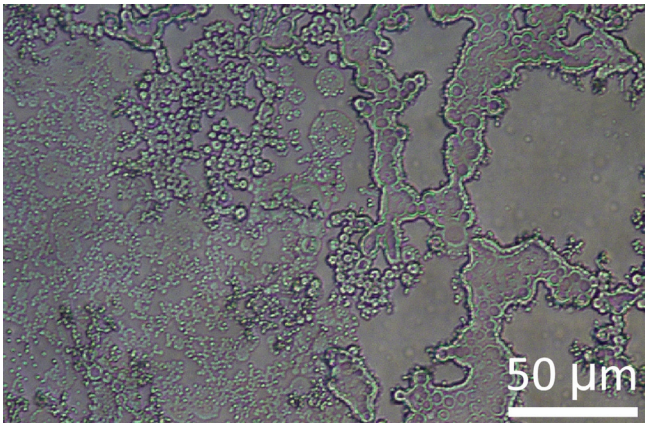

Figure 3. An optical microscopy image of material formed in a solution of composition [$CaCl_2$] = 10 mM and [PAH] = 1 mg mL^{-1} after exposure to ammonium carbonate vapor for 3 h.

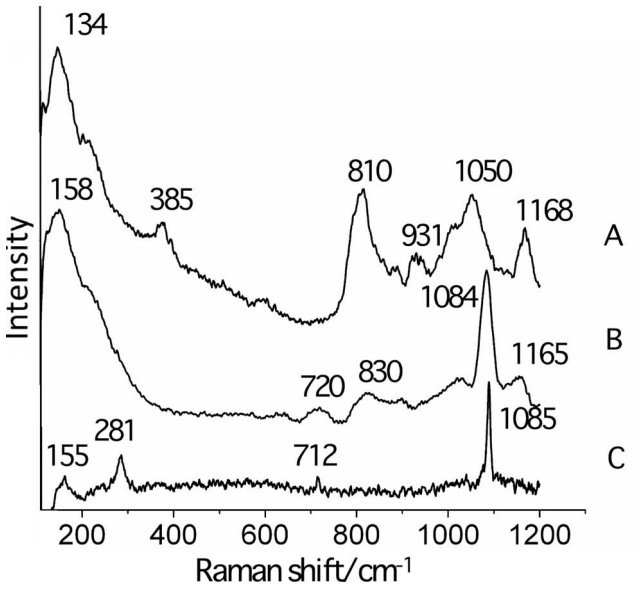

Figure 4. Raman spectra of A) PAH, B) precipitate obtained from exposure of a solution of composition [$CaCl_2$] = 10 mM and [PAH] = 1 mg mL^{-1} to ammonium carbonate vapor for 3 h, and C) a polycrystalline calcite film.

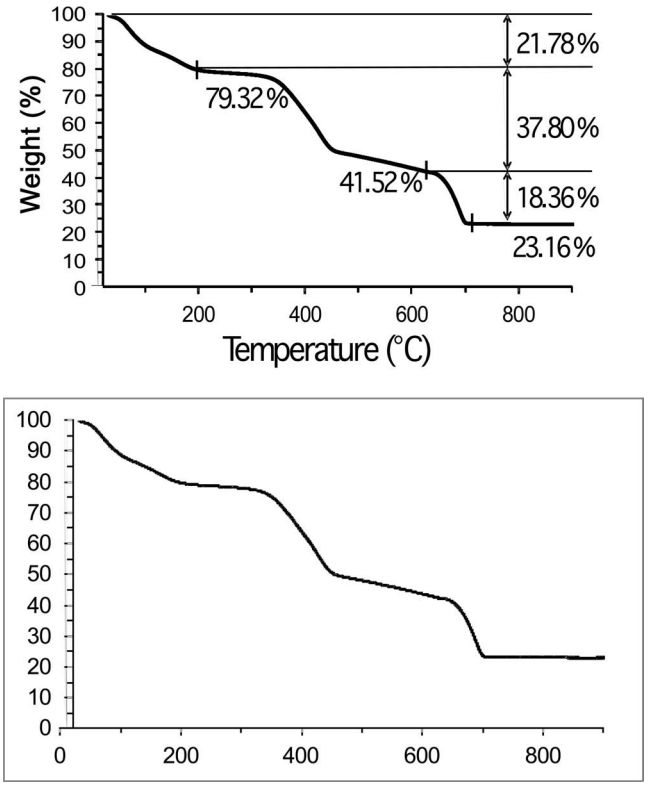

Figure 5. TGA data of precipitate obtained from exposure of a solution of composition [$CaCl_2$] = 10 mM and [PAH] = 1 mg mL^{-1} to ammonium carbonate vapor for 3 h.

experiment, thick films were deposited from a cloudy solution when the reaction had a final pH of 9.3. In contrast, only distorted calcite crystals were obtained when the experiment was repeated with initial and final pH values of ≈12, when no phase separation could occur due to the deprotonated amine group (Supporting Information Figure S2).

That the solutions comprising Ca^{2+}/PAH/CO_3^{2-} became visibly cloudy can also be attributed to the precipitation of $CaCO_3$. However, thermogravimetric analysis (TGA) and Raman investigations of the precipitates formed at early reaction times strongly support the model of phase separation, where an initial species is formed that contains Ca^{2+}/CO_3^{2-}/PAH. The Raman spectrum of the precipitate obtained from exposure of a solution of composition [$CaCl_2$] = 10 mM and [PAH] = 1 mg mL^{-1} to ammonium carbonate vapour for 3 h was compared with that of PAH alone and of a polycrystalline calcite film produced on crystallization of an amorphous film generated under the same reaction conditions (**Figure 4**). The spectrum of the precursor PAH/$CaCO_3$ species showed broad peaks at 1084 cm^{-1} (ν_1, internal CO_3^{2-} symmetric stretch mode), 720 cm^{-1} (ν_4, CO_3^{2-} symmetric bending mode), and 158 cm^{-1} (translational lattice mode), which can be attributed to ACC,[37] while the peaks at 830 cm^{-1} (C–N stretch mode) and 1165 cm^{-1} (C–H bending mode) correspond to PAH.[35] The composition of this phase was further investigated using TGA, which showed that the early stage precipitates comprised 38 wt% PAH, 42% $CaCO_3$, and 20% water (**Figure 5**). The 22% loss in weight up to 200 °C is attributed to dehydration, while the subsequent 38% weight loss up to 600 °C can be attributed to degradation of the PAH. The characteristic decomposition of calcium carbonate (42% weight loss) to calcium oxide (23%) then occurs above ≈650 °C. This can be compared with the precipitates formed in the PAH/carbonate system alone, where TGA demonstrates that the phase is composed of 37 wt% water and is therefore more hydrated in the absence of calcium ions (Supporting Information Figure S3). The decomposition profile of pure PAH was also recorded (Supporting Information Figure S3), which showed that association with carbonate or calcium ions leads to stabilization of the polymer, as shown by an increase in the decomposition temperature from ≈250 °C to ≈450 °C.

Support for a mechanism in which a microphase separation precedes crystallization was also obtained by imaging the structures present in the PAH/$CaCO_3$ reaction solution using cryo-TEM (cryoTEM, **Figure 6**). Samples taken after 30 min contained 50–100 nm particles (Figure 6A) that were prone to radiation damage such that they developed voids and then faded away upon exposure to an electron dose of 400–1200 electrons per $Å^2$ (Supporting Information Figure S4C,D). This behavior is consistent with structures that are hydrated and that contain high amounts of organic material. Further, this radiation sensitivity is very distinct from that of the surrounding amorphous ice and particles of crystalline ice, both of which remain undamaged by an electron-dose of 1600 electrons per $Å^2$ (discussed further in the Supporting Information and shown in Figure S4A,B). After 3 h, circular structures with sizes ranging from 300 nm to 1 μm were observed (Figure 6B), which were also sensitive to the electron beam (Figures 6E,F). This material was still amorphous, as shown by low dose selected area electron diffraction (LDSAED) (Figure 6B, inset). Interestingly,

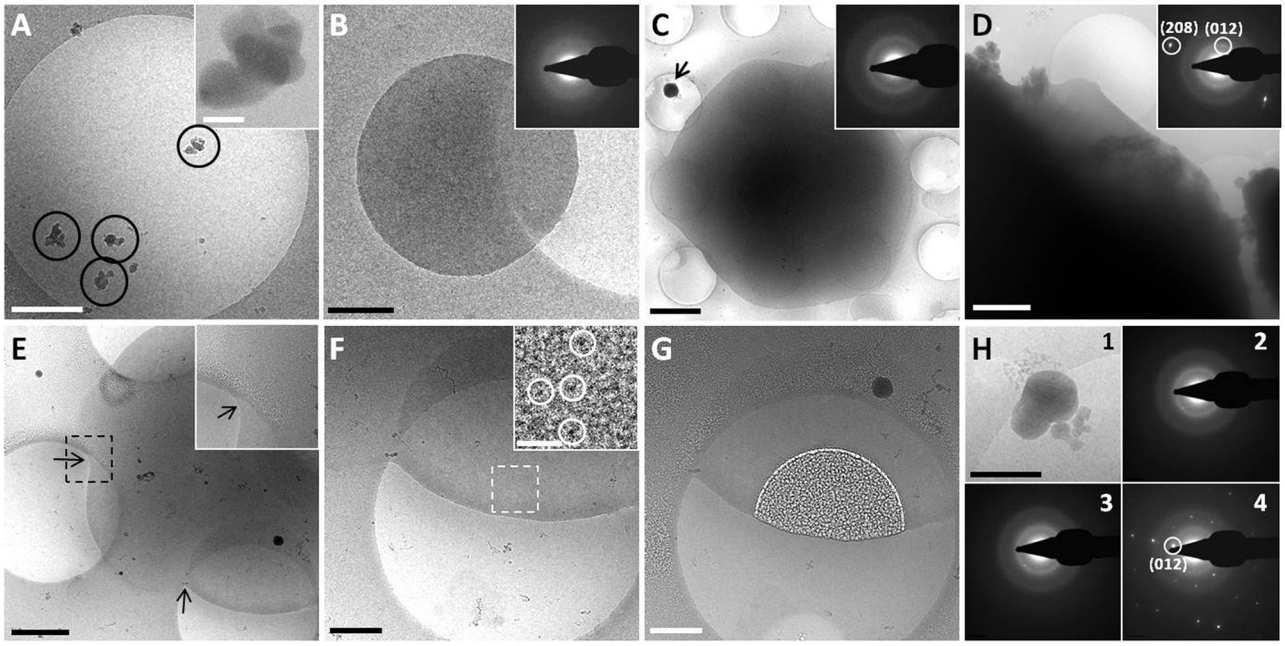

Figure 6. Cryo-TEM images of $CaCO_3$ formed in the presence of 1 mg mL^{-1} PAH at different times. A) After 30 min of reaction. Black circles highlight 50–100 nm particles (scale bar: 500 nm) and the inset shows a particle at high magnification (scale bar: 50 nm). B) 3 h of reaction, showing a droplet-like structure 1 μm in size (scale bar: 500 nm). The inset is a low-dose SAED (LDSAED) pattern, which shows that the $CaCO_3$ is amorphous. C) After 6 h, showing a $CaCO_3$ film several micrometers in size. Black arrow: ice particle contaminant (scale bar: 2 μm). The LDSAED pattern shown in the inset demonstrates that the $CaCO_3$ film is amorphous. D) A $CaCO_3$ film formed after 20 h (scale bar: 1 μm). The inset LDSAED pattern demonstrates that the film is calcite, as shown by the reflections corresponding to (012) and (208) planes. E) After 3 h, showing several droplet-like structures fusing together (black arrows). The inset shows a high magnification image of the area marked by the square (scale bar: 1 μm). F,G) Higher magnification images of (E,F) before and (G) after exposure to a dose of ≈400 electrons per $Å^2$ (scale bar: 500 nm). The inset gives a high magnification image of the area marked by the square and shows that the droplet-like structure is composed of 1 nm clusters (white circles) (scale bar: 10 nm). In (G) voids are present in the $CaCO_3$ droplet due to the radiation damage caused by the electron beam. The damage is exclusively in the droplet, and not in the ice layer. H) Quadrant 1: $CaCO_3$ particle formed after 20 h (scale bar: 500 nm). Quadrants 2–3: successive LDSAEDs taken from the particle, showing the transformation from ACC (quadrants 2 and 3) to calcite (quadrant 4) due to extended exposure to the electron beam.

these calcium carbonate structures sometimes appeared to merge together prior to vitrification, like droplets coalescing, suggesting a liquid-like behavior (Figure 6E).

Longer reaction times led to further growth of this material such that TEM grids collected after 6 h were covered by a film comprising objects of over 10 μm in diameter. These $CaCO_3$–PAH complexes typically possessed a denser core surrounded by more diffuse material (Figure 6C) and were still amorphous (Figure 6C, inset). Little change in the morphology of the film was observed after 20 h (Figure 6D), but significantly, most of the material had now transformed into calcite (Figure 6D, inset). 500 nm particles of ACC that crystallized to calcite after prolonged exposure to the electron beam were additionally present in these samples (Figure 6H), attesting to the fact that these structures were indeed composed of $CaCO_3$. Control experiments were also performed by imaging solutions of PAH, of PAH with $CaCl_2$, and of PAH with Na_2CO_3. In the former two cases only 20 nm diffuse structures were observed, which quickly disappeared upon exposure to the electron beam (Supporting Information Figure S5). The images of the solution containing PAH and Na_2CO_3 supported the observation of phase separation in this system, and films and drop-like structures 1–2 μm in diameter were observed (Supporting Information Figure S5). These structures had an internal network-like structure and were also prone to radiation damage by the electron beam. Taken together with the data provided by optical microscopy, Raman, and TGA, the cryoTEM images therefore provide good evidence of formation of an initial PAH/Ca/carbonate phase, from which calcium carbonate subsequently crystallizes.

3. Discussion

The experiments therefore demonstrate that PAH, which is positively charged at the pH at which crystallization occurs, can strongly influence the precipitation of calcium carbonate and induce significant changes in calcite morphologies. This result is perhaps immediately surprising given the prevailing understanding that positively charged additives exert a relatively weak effect on $CaCO_3$ precipitation. This viewpoint is supported by the fact that very few studies of additive-directed calcium carbonate growth have been reported with positively charged additives as compared with their negatively charged counterparts. Further, these studies, such as those with lysine,[38] poly-L-lysine,[39,40] or with a positively-charged 16-residue peptide[41] tend to show relatively minor changes in morphology. It has been noted, however, that amine side-groups have a tendency to

stabilize vaterite with respect to calcite.[29,30] As a notable exception to this, aggregates of poly(propylene imine) dendrimers that were modified with octadecylamine were active in stabilizing ACC, a behavior that was attributed to their structural rigidity.[42]

The mechanism by which PAH directs the formation of fibers and films does, however, provide a basis for rationalizing its behavior. Indeed, it is also valuable to note that PAH induces the formation of calcium carbonate thin films and fibers that are identical in structure and morphology to those generated in the $CaCO_3$/PAsp (PAA) "PILP" system, albeit at slightly higher polymer concentrations (10–100 μg mL^{-1} of PAA or PAsp are typically used to achieve similar results.[43,44]) That higher concentrations of polymer are required in the $CaCO_3$/PAH as compared with the $CaCO_3$/PAsp (PAA) system suggests weaker polymer/counter-ion interaction at the working pH of ≈9. This may reflect the degree of protonation of the polymers as PAH is only 50% protonated at pH 9.5, while PAsp/PAA are fully deprotonated at this pH value.[36] We therefore suggest that the effect of PAH can be attributed to the fact that it undergoes a microphase separation driven by the carbonate ions rather than a strong specific binding of the amine groups with the developing crystal. This generates highly hydrated Ca^{2+}/CO_3^{2-}/PAH species that gradually convert to ACC with time, before ultimately crystallizing (**Figure 7**). This mechanism therefore mirrors that believed to occur in the PAsp/PAA $CaCO_3$ system,[26] where PAA phase separates in the presence of Ca^{2+} ions,[45] and the presence of carbonate ions appears to enable this process to occur at lower polymer concentrations.[26] This emphasises that it is the formation of hydrated Ca^{2+}/polymer/CO_3^{2-} droplets that is key to this process, rather than a specific polymer/mineral interaction. These droplets then merge to generate the thin films and fibers that provide an immediate fingerprint of this crystallization mechanism.

Adding to the discussion, Wolf et al. have recently observed the formation of $CaCO_3$ thin films in the presence of the acidic protein ovalbumin, where they suggest that a liquid amorphous calcium carbonate (LACC) phase forms in the presence of the polymer.[46] The LACC is stabilized due to electrostatic and depletion factors as the "droplets" are negatively charged, and their formation markedly reduced the free Ca^{2+} concentration in solution (depletion stabilization), thereby reducing the rate of crystallization. Similar factors are likely to operate in the $CaCO_3$/PAH system as indicated by the fact that the droplets produced exhibit positive surface charges of 12 mV, as determined by zeta

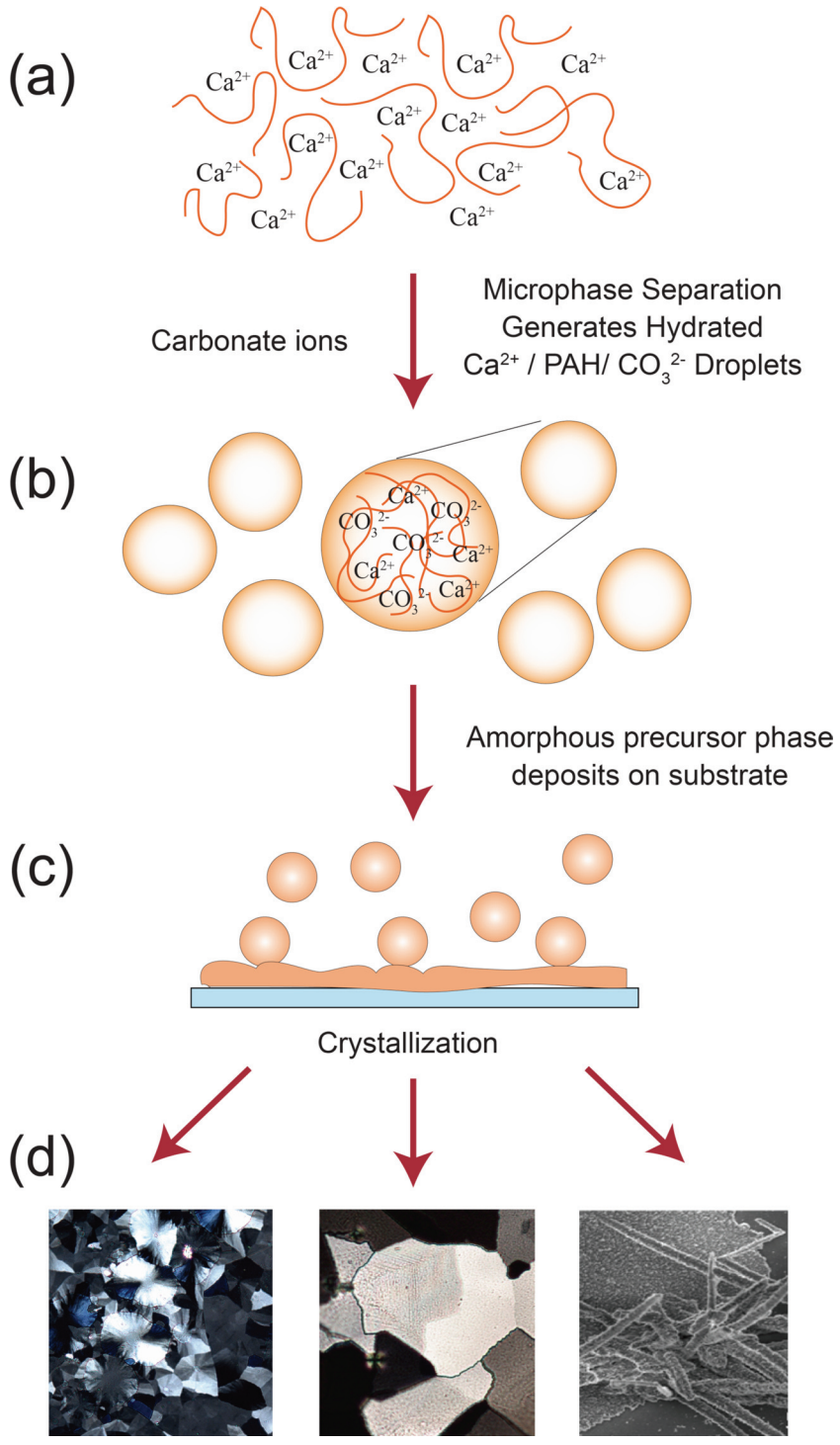

Figure 7. Schematic diagram of the formation of thin films and fibers of calcium carbonate in the presence of PAH. A solution of PAH and calcium ions (a) are exposed to ammonium carbonate vapor, leading to separation of droplets of a hydrated $Ca^{2+}/PAH/CO_3^{2-}$ phase (b). The droplets grow and deposit on a substrate whether they coalesce to form thin films and fibrous structures (c). Subsequent crystallization generates uniform thin films of calcium carbonate that comprise either polycrystalline or single crystal calcite domains, with which calcite fibers are often associated (d).

potential measurements (Supporting Information Figure S6) of droplets present in the reaction solution after 3 h.

Having established that microphase separation can provide a route to producing $CaCO_3$ crystals with non-crystallographic structures, a significant question remains. Is this relevant to calcium carbonate biomineralization, as has been suggested,[26] and could an analogous effect be achieved with the proteins present within $CaCO_3$ biominerals? The macromolecules associated with $CaCO_3$ biominerals represent a rather special class of proteins. They are classified as "highly acidic", containing from ≈20% up to 40–50 mol% of glutamic and aspartic acid.[8,47–49] These residues are present as negatively charged domains heterogeneously distributed along the chain and exist together with domains of positive amino acids and a range of other polar or hydrophobic groups. Thus, in common with simple polyelectrolytes, proteins comprising 50% glutamic and aspartic acid would be predicted to strongly associate with Ca^{2+} ions, which could conceivably lead to microphase separation if they were sufficiently flexible. Further, recent studies of a number of proteins extracted from $CaCO_3$ biominerals have shown that they can be fully or partially disordered, and that they fall into the category of intrinsically disordered proteins (IDPs).[50–53] Such proteins can be fully functional in an unfolded state, and it has been proposed that this conformational freedom may enable them to undergo a disorder-to-order transformation on binding to a target surface such as calcite or ACC.[51] Based on their chemistry alone, it is therefore conceivable that highly acidic biomacromolecules could be active both in driving a phase separation, thereby changing crystal morphologies and textures. The positively charged residues lysine and arginine in these proteins are unlikely to support phase separation as they are of low abundance and poly-L-lysine does not phase separate in the presence of carbonate ions.[54]

Running counter to this suggestion, however, are some observations of mineralization in biological systems where it appears that amorphous calcium carbonate (ACC) and amorphous calcium phosphate (ACP) are present as well-defined granules prior to transfer to the mineralization site.[27,55,56] In considering the possibility that phase separation can participate in biogenic mineralization, there is of course one biomineralization process where phase separation certainly does play an integral part: silicification in diatoms. Isolation of the macromolecules entrapped within diatom silica has yielded the "silaffins", a category of highly phosphorylated proteins functionalized by long-chain polyamines.[57,58] In vitro experiments have shown that silaffins can undergo microphase separation in the presence of silicic acid, thereby forming droplets which can act as a template for pattern formation in the diatom wall.[34,59]

4. Conclusions

In conclusion, we have demonstrated that poly(allylamine hydrochloride) can strongly influence calcium carbonate precipitation and induce the formation of calcite thin films and fibers. This result therefore challenges the current understanding that such an effect is unique to acidic macromolecules. Our results suggest that it is a counter-ion induced phase separation, which causes the formation of the thin films and fibers characteristic of this growth mechanism, which is consistent with the observation of similar morphological effects in a number of polyelectrolyte/crystal systems. For example, DNA,[60] ovalbulmin[46] and a calcification-associated peptide,[61] have been shown to support the formation of thin films of $CaCO_3$, the infiltration of calcium phosphate precipitated in the presence of poly(aspartic acid) into the nanosized gaps in collagen pores was considered evidence of a PILP phase,[62,63] while fibers and limited film formation was induced by poly(acrylic acid) in the barium and strontium carbonate systems.[64] The PILP strategy has also been successfully applied to the crystallization of single component molecular crystals; crystalline thin films and spherical particles of a number of amino acids were formed on precipitation from water/ethanol solutions in the presence of oppositely charged polyelectrolytes.[65,66] While there is no current evidence that the ability of PAH to direct $CaCO_3$ precipitation is relevant to $CaCO_3$ biomineralization, it is certainly possible that the most acidic biomacromolecules could direct a microphase separation. In demonstrating for the first time that a positively charged polymer can lead to the formation of a PILP phase, we therefore highlight the opportunity for using such a counter-ion-induced phase separation as a synthetic tool and believe that this method could be used to create a wide range of minerals with non-crystallographic morphologies.

5. Experimental Section

Calcium Carbonate Precipitation: Calcium carbonate was precipitated in the presence of poly(allylamine hydrochloride) (PAH) (M_w 56 KDa Aldrich) under a range of solution concentrations, and the progress of the reaction was investigated as a function of time and pH. PAH was added to a 10 mM $CaCl_2$ solution to give a concentration of 1 mg mL^{-1} and a 10 mL aliquot was transferred to a Petri dish. A glass slide that had been cleaned with Piranha solution (70 vol% sulphuric acid, 30 vol% hydrogen peroxide) was then placed upright in the dish, which was finally covered with Parafilm. The Parafilm was pierced four times with a needle and the dish was placed in a sealed desiccator, along with a dish containing 5 g of ammonium carbonate, which had also been covered with Parafilm and pierced four times with a needle. Crystallization was then allowed to proceed over periods ranging from 30 min to 6 days. The initial pH of the solution ranged between ≈4.2 and 7 depending on the PAH concentration, and increased to ≈9.5 at the termination of crystal growth. After this time the glass slides were removed from solution, washed with ethanol, and allowed to dry at room temperature. Control experiments were also performed using identical procedures to those described above, but in the absence of PAH.

In order to investigate the phase separation occurring at early stages of the reaction, the precipitate formed in a 3 h reaction solution ([$CaCl_2$] = 10 mM, [PAH] = 1 mg mL^{-1}) was isolated by centrifugation (15 min at 11000 rpm). It was subsequently washed with ethanol and was again isolated by centrifugation. This material was then allowed to dry in air overnight, and was then analyzed using Raman microscopy and TGA (TA Instruments, SDT Q600 Simultaneous TGA/DSC) with 5 °C min^{-1} heating rate under air. The spectra obtained were compared with those from a control sample which had been prepared in the absence of Ca^{2+} ions by mixing 10 mM Na_2CO_3 with 1 mg mL^{-1} PAH and adjusting the pH level to 9.0. The effect of the solution pH on the precipitation of calcium carbonate was also studied by mixing the initial $CaCl_2$ and Na_2CO_3 solutions at different starting pH values. A 20 mM Na_2CO_3 solution containing 1 mg mL^{-1} PAH was slowly mixed with 20 mM $CaCl_2$ by dropwise addition of the $CaCl_2$ solution, to give final concentrations of 10 mM Na_2CO_3, 0.5 mg mL^{-1} PAH, and 10 mM $CaCl_2$. The initial pH of the solutions was varied from 4 to 12 to give different final pH values.

Characterization of the Calcium Carbonate Precipitates: The calcium carbonate formed on the glass slide immersed in the precipitation solution was investigated using a range of analytical techniques including field emission gun scanning electron microscopy (FEGSEM), TEM (FEGTEM), micro-Raman microscopy, and polarized optical microscopy. FEGSEM provided detailed morphological information, and samples were prepared by mounting the glass slides on SEM stubs with adhesive carbon pads, and sputter-coating them with 10 nm Pt/Pd (80/20) using an agar high-resolution sputter coater. Samples were then examined using a LEO 1530 Gemini FEGSEM operating at 3.00 kV with an in-lens detector. Optical microscopy was used to characterize the morphology of the precipitates and examination between crossed polarizers provided information on their single crystal/polycrystalline/amorphous structures. Micro-Raman spectroscopy and electron diffraction were used to determine the $CaCO_3$ polymorphs present in the samples. Raman measurements were carried out using a Renishaw 2000 inVia-Raman microscope using a 785 nm diode laser as the excitation source. The laser was focussed onto the sample using a 50× (numerical aperture NA 0.75) objective, enabling the individual structure of the particles to be determined. Fibers were investigated by TEM by scraping them off the supporting glass slides and transferring to a formvar-carbon-coated Cu TEM grid. The samples were then examined at 200 kV in a FEI Tecnai TF20 FEG-TEM and diffraction patterns were obtained using selected area electron diffraction techniques (SAED). Zeta-potential measurements were also performed to determine the charge of the precursor species and were obtained electrophoretic mobilities using a Malvern Zetasizer NanoZS Instrument equipped with a 4 mW He-Ne solid-state laser operating at 633 nm.

Cryo-TEM: A vitrification robot (FEI Vitrobot Mark III) equipped with a humidity- and temperature-controlled glove box was used to prepare the cryo-TEM samples. Cryo-TEM grids, R2/2 Quantifoil Au Jena grids, were purchased from Quantifoil Micro Tools GmbH and before the vitrification procedure they were surface plasma treated using a Cressington 208 carbon coater. 3 µL of reaction solution was taken from the reaction vial and applied to the Au grid inside the vitrobot chamber, at 100% humidity and 20 °C. Subsequently, the grid was blotted for 2 s with filter paper and plunge-frozen in melting ethane at liquid nitrogen temperature. The samples were then kept in liquid nitrogen and loaded into the cryo-TEM apparatus. Cryo-TEM experiments were carried out on the TU/e CryoTitan (FEI) (www.cryotem.nl) equipped with a field emission gun operating at 300 kV and with a postcolumn Gatan energy filter. Images were recorded using a 2000 × 2000 Gatan charge-coupled device (CCD) camera.

Supporting Information

Supporting Information is available from the Wiley Online Library or from the author.

Acknowledgements

The authors thank the EPSRC for financial support via grants EP/E037364/2 and EP/H005374/1 (Y.Y.K. and B.C.). They also thank the Dutch Science Foundation, NWO, The Netherlands, for financial support through a VICI grant (F.N. and N.A.J.M.S.). H.L. is most grateful to the DAAD for funding his visit to the UK.

Received: October 4, 2011
Revised: November 2, 2011
Published online: January 9, 2012

[1] F. C. Meldrum, H. Colfen, *Chem. Rev.* **2008**, *108*, 4332.
[2] B. Wucher, W. Yue, A. N. Kulak, F. C. Meldrum, *Chem. Mater.* **2007**, *19*, 1111.
[3] H. A. Lowenstam, S. Weiner, *On Biomineralization*, Oxford University Press, New York **1989**.
[4] N. Sommerdijk, G. de With, *Chem. Rev.* **2008**, *108*, 4499.
[5] G. Falini, S. Albeck, S. Weiner, L. Addadi, *Science* **1996**, *271*, 67.
[6] A. M. Belcher, X. H. Wu, R. J. Christensen, P. K. Hansma, G. D. Stucky, D. E. Morse, *Nature* **1996**, *381*, 56.
[7] L. Addadi, S. Weiner, *Proc. Natl. Acad. Sci. USA* **1985**, *82*, 4110.
[8] B. A. Gotliv, L. Addadi, S. Weiner, *ChemBioChem* **2003**, *4*, 522.
[9] H. Endo, Y. Takagi, N. Ozaki, T. Kogure, T. Watanabe, *Biochem. J.* **2004**, *384*, 159.
[10] M. Michenfelder, G. Fu, C. Lawrence, J. C. Weaver, B. A. Wustman, L. Taranto, J. S. Evans, D. E. Morsel, *Biopolymers* **2003**, *70*, 522.
[11] A. Sato, S. Nagasaka, K. Furihata, S. Nagata, I. Arai, K. Saruwatari, T. Kogure, S. Sakuda, H. Nagasawa, *Nat. Chem. Biol.* **2011**, *7*, 197.
[12] T. Samata, N. Hayashi, M. Kono, K. Hasegawa, C. Horita, S. Akera, *FEBS Lett.* **1999**, *462*, 225.
[13] J. S. Evans, *Chem. Rev.* **2008**, *108*, 4455.
[14] K. A. Piez, *Science* **1961**, *134*, 841.
[15] P. E. Hare, *Science* **1963**, *139*, 216.
[16] K. Simkiss, *Comp. Biochem. Phys.* **1965**, *16*, 427.
[17] D. F. Travis, C. J. Francois, L. C. Bonar, M. J. Glimcher, *J. Ultrastruct. Res.* **1967**, *18*, 519.
[18] S. Weiner, *Calcif. Tissue Int.* **1979**, *29*, 163.
[19] B. R. Heywood, S. Mann, *Adv. Mater.* **1994**, *6*, 9.
[20] J. Aizenberg, A. J. Black, G. H. Whitesides, *J. Am. Chem. Soc.* **1999**, *121*, 4500.
[21] J. M. Didymus, P. Oliver, S. Mann, *J. Chem. Soc. Faraday Trans.* **1993**, *89*, 2891.
[22] S. Elhadj, E. A. Salter, A. Wierzbicki, J. J. De Yoreo, N. Han, P. M. Dove, *Cryst. Growth Des.* **2006**, *6*, 197.
[23] T. X. Wang, H. Colfen, M. Antonietti, *J. Am. Chem. Soc.* **2005**, *127*, 3246.
[24] J. Donners, R. J. M. Nolte, N. Sommerdijk, *J. Am. Chem. Soc.* **2002**, *124*, 9700.
[25] S. H. Yu, H. Cölfen, *J. Mater. Chem.* **2004**, *14*, 2124.
[26] L. B. Gower, *Chem. Rev.* **2008**, *108*, 4551.
[27] E. Beniash, J. Aizenberg, L. Addadi, S. Weiner, *Proc. R. Soc.* **1997**, *264*, 461.
[28] C. L. Freeman, J. H. Harding, D. Quigley, P. M. Rodger, *J. Phys. Chem. C* **2011**, *115*, 8175.
[29] A. W. Xu, M. Antonietti, H. Colfen, Y. P. Fang, *Adv. Funct. Mater.* **2006**, *16*, 903.
[30] Q. Yu, H. D. Ou, R. Q. Song, A. W. Xu, *J. Cryst. Growth* **2006**, *286*, 178.
[31] N. Nassif, N. Pinna, N. Gehrke, M. Antonietti, C. Jager, H. Colfen, *Proc. Natl. Acad. Sci. USA* **2005**, *102*, 12653.
[32] M. J. Olszta, S. Gajjeraman, M. Kaufman, L. B. Gower, *Chem. Mater.* **2004**, *16*, 2355.
[33] K. Kolasinski, *Curr. Opin. Solid State Mater. Sci.* **2006**, *10*, 182.
[34] E. Brunner, K. Lutz, M. Sumper, *Phys. Chem. Chem. Phys.* **2004**, *6*, 854.
[35] H. Daiguji, E. Matsuoka, S. Muto, *Soft Matter* **2010**, *6*, 1892.
[36] A. I. Petrov, A. A. Antipov, G. B. Sukhorukov, *Macromolecules* **2003**, *36*, 10079.
[37] R. S. K. Lam, J. M. Charnock, A. Lennie, F. C. Meldrum, *CrystEngComm* **2007**, *9*, 1226.
[38] A. J. Xie, Y. H. Shen, C. Y. Zhang, Z. W. Yuan, X. M. Zhu, Y. M. Yang, *J. Cryst. Growth* **2005**, *285*, 436.
[39] B. Njegic-Dzakula, L. Brecevic, G. Falini, D. Kralj, *Cryst. Growth Des.* **2009**, *9*, 2425.
[40] Y. Yao, W. Y. Dong, S. M. Zhu, X. H. Yu, D. Y. Yan, *Langmuir* **2009**, *25*, 13238.
[41] D. L. Masica, S. B. Schrier, E. A. Specht, J. J. Gray, *J. Am. Chem. Soc.* **2010**, *132*, 12252.
[42] J. Donners, B. R. Heywood, E. W. Meijer, R. J. M. Nolte, N. Sommerdijk, *Chem.-Eur. J.* **2002**, *8*, 2561.

[43] X. G. Cheng, P. L. Varona, M. J. Olszta, L. B. Gower, *J. Cryst. Growth* **2007**, *307*, 395.
[44] E. DiMasi, S. Y. Kwak, F. F. Amos, M. J. Olszta, D. Lush, L. B. Gower, *Phys. Rev. Lett.* **2006**, *97*, 4.
[45] M. A. V. Axelos, M. M. Mestdagh, J. Francois, *Macromolecules* **1994**, *27*, 6594.
[46] S. E. Wolf, J. Leiterer, B. Pipich, R. Barrea, F. Emmerling, W. Tremel, *J. Am. Chem. Soc.* **2011**, *133*, 12642.
[47] S. C. Benson, N. C. Benson, F. Wilt, *J. Cell Biol.* **1986**, *102*, 1878.
[48] S. Weiner, *Am. Zool.* **1984**, *24*, 945.
[49] S. Weiner, *Crit. Rev. Biochem.* **1986**, *20*, 365.
[50] F. F. Amos, E. Destine, C. B. Ponce, J. S. Evans, *Cryst. Growth Des.* **2010**, *10*, 4211.
[51] K. Delak, S. Collino, J. S. Evans, *Biochemistry* **2009**, *48*, 3669.
[52] K. Delak, C. Harcup, R. Lakshminarayanan, Z. Sun, Y. W. Fan, J. Moradian-Oldak, J. S. Evans, *Biochemistry* **2009**, *48*, 2272.
[53] T. M. Kaplon, G. Rymarczyk, M. Nocula-Lugowska, M. Jakob, M. Kochman, M. Lisowski, Z. Szewczuk, A. Ozyhar, *Biomacromolecules* **2008**, *9*, 2118.
[54] B. J. McKenna, H. Birkedal, M. H. Bartl, T. J. Deming, G. D. Stucky, *Angew. Chem. Int. Ed.* **2004**, *43*, 5652.
[55] E. Beniash, L. Addadi, S. Weiner, *J. Struct. Biol.* **1999**, *125*, 50.
[56] J. Mahamid, A. Sharir, D. Gur, E. Zelzer, L. Addadi, S. Weiner, *J. Struct. Biol.* **2011**, *174*, 527.
[57] N. Kroger, N. Poulsen, *Annu. Rev. Genet.* **2008**, *42*, 83.
[58] M. Sumper, E. Brunner, *Adv. Funct. Mater.* **2006**, *16*, 17.
[59] N. Kroger, S. Lorenz, E. Brunner, M. Sumper, *Science* **2002**, *298*, 584.
[60] N. Sommerdijk, E. N. M. van Leeuwen, M. R. J. Vos, J. A. Jansen, *CrystEngComm* **2007**, *9*, 1209.
[61] A. Sugawara, T. Nishimura, Y. Yamamoto, H. Inoue, H. Nagasawa, T. Kato, *Angew. Chem. Int. Ed.* **2006**, *45*, 2876.
[62] M. J. Olszta, X. G. Cheng, S. S. Jee, R. Kumar, Y. Y. Kim, M. J. Kaufman, E. P. Douglas, L. B. Gower, *Mat. Sci. Eng. R* **2007**, *58*, 77.
[63] F. Nudelman, K. Pieterse, A. George, P. H. H. Bomans, H. Friedrich, L. J. Brylka, P. A. J. Hilbers, G. de With, N. Sommerdijk, *Nat. Mater.* **2010**, *9*, 1004.
[64] S. J. Homeijer, M. J. Olszta, R. A. Barrett, L. B. Gower, *J. Cryst. Growth* **2008**, *310*, 2938.
[65] S. Wohlrab, H. Cölfen, M. Antonietti, *Angew. Chem. Int. Ed.* **2005**, *44*, 4087.
[66] Y. Jiang, H. Gong, D. Volkmer, L. B. Gower, H. Cölfen, *Adv. Mater.* **2011**, *23*, 3548.